A Laboratory Simulation of Convective Vortices

D. E. FITZJARRALD[1]

Dept. of Meteorology, University of California, Los Angeles 90024

(Manuscript received 24 October 1972, in revised form 21 February 1973)

ABSTRACT

An experiment has been constructed which yields a vortex flow similar in many respects to atmospheric dust devils. Measurements were made of air velocity and temperature in the vortex core. These results were compared with a theoretical model of the flow, with velocities measured in real dust devils, and with the results of previous researchers who used a non-convective vortex. Observations were made of the different types of vortex flows found in the chamber and their dependence on the controlling parameters.

1. Introduction

Because of the transient nature of atmospheric vortices, field observations of the smallest—water spouts and dust devils—are extremely difficult. The complex interdependence between different regions of the flow fields within the vortex makes formulation of adequate theoretical models an arduous task (Long, 1958; Lewellen, 1962; Kuo, 1966; Barcilon, 1967a, b; Carrier *et al.*, 1971; Serrin, 1972). For these reasons and because of the ubiquitous presence of vortex phenomena in the atmosphere, laboratory simulations have been performed by many researchers. The studies range from simple, qualitative demonstrations (Turner and Lilly, 1963; Barcilon, 1967a) to more elaborate quantitative experiments (Maxworthy, 1964; Ying and Chang, 1970; Wan and Chang, 1972; Ward, 1970; Barcilon, 1967b).

Even though all atmospheric vortices are driven by convection, either directly in the case of the dust devil or by cumulus convection in the case of waterspouts and tornadoes, the most complete laboratory simulations have used mechanical non-convective means to maintain the motion. The most common experimental technique utilizes an exhaust fan to create an updraft at the center of the chamber. Onrushing fluid at the perimeter is given a tangential velocity component and spirals in toward the center, forming a concentrated tornado-like vortex. This arrangement is obviously not well suited for studying the dust-devil-type vortex, since the thermal field and driving mechanism are not utilized at all. Even for tornadoes and waterspouts, which may be assumed to be driven by a larger scale convection, the updraft mechanism introduces an unwanted upper boundary condition not present in atmospheric vortices. The effect of varying the updraft area is noted by Ying and Chang, and studied in detail by Ward who finds significant difference in the observed vortex, depending on the ratio of updraft area to inflow area.

2. Description of apparatus

In order to eliminate the difficulty associated with the upper boundary and simulate the thermal properties of a dust devil vortex, an apparatus was constructed using the simplest boundary conditions. A circular, uniformly heated aluminum plate formed the lower boundary, and 20 plexiglass windows were arranged around the circumference to impart a tangential velocity component to the inrushing air. A sketch of the apparatus is shown in Fig. 1.

Tilted windows were chosen to provide swirl at the inlet instead of rotating screens used in previous studies (Barcilon, 1967b; Ying and Chang, 1970; Ward, 1970). The use of stationary windows eliminates the need for rotating machinery, makes flow visualization simpler, and facilitates the operation of optical velocity measuring devices. The price paid for this simplification, however, is an amount of indeterminacy in the imposed swirl condition. Both the velocity and vorticity become rather complex at the outer boundary because of the effect of the windows. The outer boundary of the chamber is far enough away from the vortex so that this effect is not great, however. No significant effect of the windows on the vortex was observed, except the desired one of creating swirl.

The vortex formed at the center of the chamber was made visible by means of smoke introduced into the desired portion of the flow field by means of a glass tube. A laser Doppler velocity measuring system was constructed and used to measure the velocity of con-

[1] Present affiliation: Institute of Geophysics and Planetary Physics, University of California, Los Angeles.

centrated smoke in the vortex core. With this instrument one component of velocity could be measured at a fixed point in the test chamber whenever the smoke was dense enough to provide sufficient optical scattering material. Temperatures were measured with an array of four glass bead thermistors arranged to give a vertical profile of temperature in the chamber. [For a complete description of the velocity and temperature measurement systems and the test chamber, see Fitzjarrald (1972).]

3. Scaling the experimental results

Measurements made in the test chamber must be scaled properly in order to be compared with field data and applicable theories. The experiment has only two independently controllable parameters. The plate temperature T_p determines the buoyant acceleration $[g(T_p-T_\infty)/T_\infty]$, and the angle of the inlet windows determines the angle of the streamlines at the inlet $[\theta=\tan^{-1}(V_\infty/U_\infty)]$. Here T_∞, V_∞ and U_∞ are the temperature, tangential velocity and radial velocity at the inlet.

The length scale is the radius of the heated plate, R. The relevant velocity scale is the convective velocity $[V^2=gR(T_p-T_\infty)/T_\infty]$ (Kuo, 1966). An applicable stability parameter is given by Barcilon (1967a):

$$\Lambda=Zg(T_p-T_\infty)/(T_\infty V_\infty^2),$$

where

$$Z=\sqrt{\epsilon}R, \quad \epsilon=\mathrm{Re}^{-1}=\nu/(V_\infty R).$$

The parameter Λ is a kind of Richardson number or inverse Froude number and represents the ratio of potential to kinetic energy in the boundary layer.

However, in the present experiment the velocity at the outer boundary cannot be independently specified. In order to minimize uncertainties the results will be presented using a stability parameter:

$$S=\left(\frac{T_p-T_\infty}{T_\infty}\right)\Big/\tan^2\theta=\left(\frac{T_p-T_\infty}{T_\infty}\right)\Big/(V_\infty/U_\infty)^2,$$

which is composed of only the independent parameters. Measurement of V_∞ will be made in order to relate S with Λ for comparison with field data and previous non-convective laboratory simulations.

4. Velocity measurements

The laser Doppler velocity meter used to measure vortex velocities presented an output which was linear and unaffected by temperature perturbations. However, its limitations imposed severe restraints on the measurements which could be made. Because the measuring volume was fixed in space and the vortex free to move about in the chamber, it was not possible to determine what radial position of the vortex was being examined. The experimental procedure was to determine the peak value of velocity as the vortex core passed through the measuring volume. A sufficient number of peaks were recorded to insure that the value obtained was representative of the operating conditions.

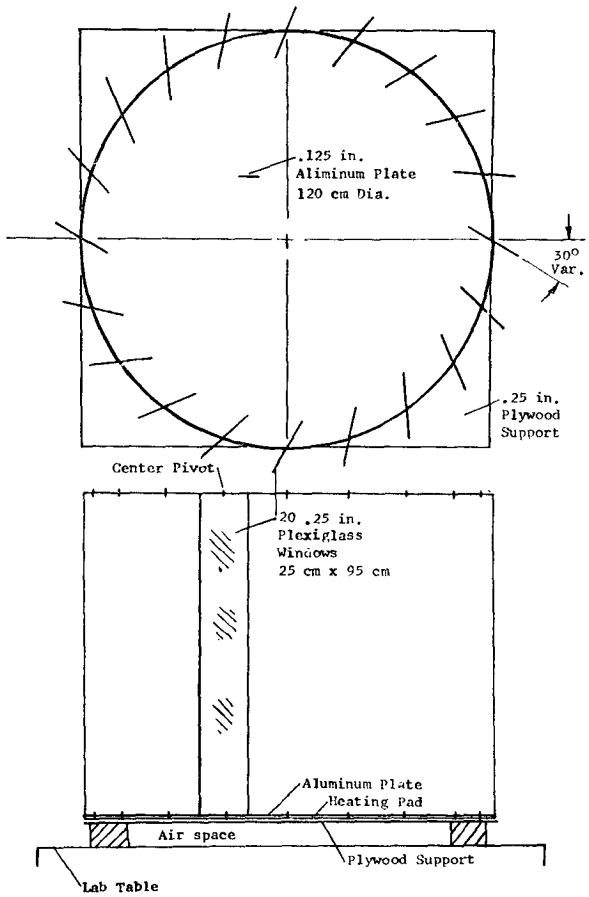

FIG. 1. Sketch of laboratory test chamber.

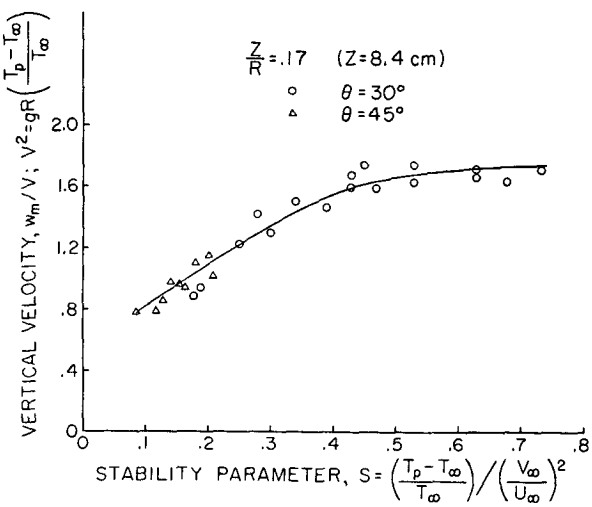

FIG. 2. Vertical velocity vs stability parameter S, measured at $Z/R=0.17$. Two values of inlet window were used, $\theta=30°$, 45°.

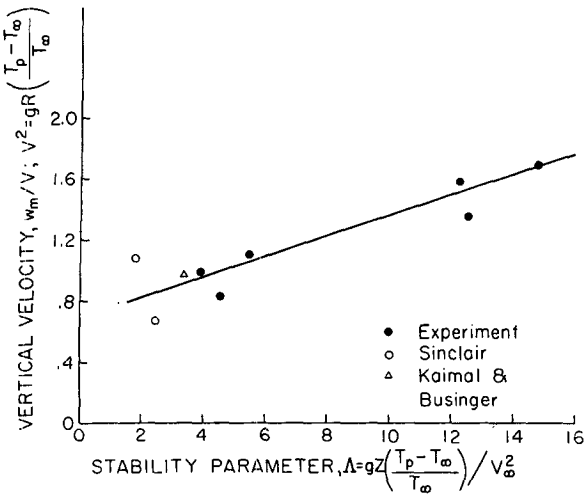

FIG. 3. Vertical velocity vs stability parameter Λ, using the experimental data shown in Table 2 to calculate the stability parameter. Shown for comparison are field measurements of Sinclair and of Kaimal and Businger.

An example of using this velocity measuring technique is shown in Fig. 2, which shows the maximum vertical velocity W_m in the vortex core at height $Z/R=0.17$. The values are non-dimensionalized by the velocity scale V discussed above and plotted versus the stability parameter S. Each point represents the peak value of velocity recorded for a given period of time, usually exceeding 15 min. The scatter inherent in using this method can be seen. The choice of S as stability parameter is given support by noting that data obtained at different plate temperatures and window angles fall approximately on the same curve. The magnitude of the velocity indicates that the proper velocity scale has been used. We see that for $S>0.4$ the scaled velocity remains constant. The velocity always increases as the plate temperature is increased, but for this range of S the increase is just the same as V.

The data presented in Fig. 2 can be related to the parameter Λ by determining V_∞. This was done using a hot-wire anemometer (Fitzjarrald, 1972). The comparison between S and Λ is shown in Table 1. The values for V_∞ represent the tangential component of inflow velocity for the lowest 30 cm and are averaged over an 8-min interval.

Using the results of Table 1 the vertical velocities of Fig. 2 are plotted against Λ in Fig. 3. Also shown in Fig. 3 are three points representing the data from real dust devils by Sinclair (1966) and Kaimal and Businger (1970). In order to make the comparison with the laboratory data, Λ and V were calculated for the field conditions reported.

A potential vortex $vr=$constant was fitted to the outer portion of the dust devil in order to calculate $\epsilon=\nu/(V_\infty R)$, and the horizontal scale length corresponding to R was taken as the radius at which the tangential velocity decreased to 0.1 of its maximum value.

TABLE 1. Stability parameters for the experiments.

T_p-T_∞ (°C)	θ (deg)	V_∞ (cm sec^{-1})	ϵ	S	Λ
31	45	5.3	$\frac{1}{1560}$	0.10	4.6
42	45	6.4	$\frac{1}{1880}$	0.14	3.9
60	45	6.4	$\frac{1}{1880}$	0.20	5.5
31	30	3 5	$\frac{1}{1030}$	0.31	12.8
42	30	4.0	$\frac{1}{1180}$	0.42	12.5
60	30	4.3	$\frac{1}{1270}$	0.60	15.3

The vertical scale height calculated using the relation $Z=\sqrt{\epsilon}R$ is at least two orders of magnitude too small for the field observations ($Z=\sqrt{\epsilon}R\approx 2.8$ cm). For this reason the vertical scale height Z was taken to be the same as the vortex radius close to the ground. This assumption is supported by the theoretical work of Barcilon (1967a). In order to relate the maximum temperature excess recorded at some height above the ground in the field observations with the quantity T_p-T_∞ observed in the lab, reference was made to the temperature measurements to be described below. Since the maximum temperature excess $T(z)-T_\infty$ measured in the laboratory vortex was approximately 1/3 of T_p-T_∞, the vortex temperatures from the field observations were tripled. Table 2 shows the results of the calculation.

While this procedure is obviously quite rough, and using only three events is not at all representative of the great variation seen in nature, the field data agree well with the laboratory points. For these three dust

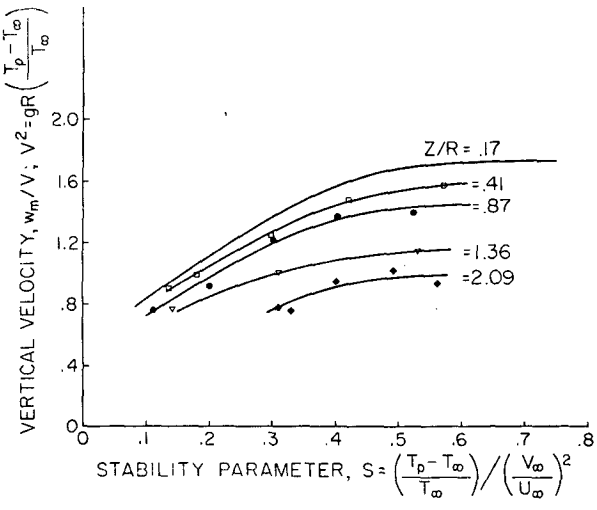

FIG. 4. Vertical velocity vs stability parameter S measured at $Z/R=0.17, 0.41, 0.87, 1.36, 2.09$.

TABLE 2. Stability parameters for field data.

	V (m sec^{-1})	W_m/V	ϵ	R (m)	Λ
Sinclair no. 1	7.1	1.06	$2.2.10^{-7}$	3.5	1.8
Sinclair no. 2	8.7	0.63	$1.5.10^{-7}$	5.0	2.4
Kaimal and Businger	4.2	0.95	$4.2.10^{-7}$	4.0	3.3

devils at least, the closest simulation will be obtained at small instability, $S \approx 0.15$. With more field data we would expect to find some dust devils corresponding to higher instabilities.

Measurements of vertical velocity at additional heights were made and are shown in Fig. 4. The curves for different values of Z/R are seen to have similar form to that for the lowest level, $Z/R=0.17$. We would expect them all to show a similar dependence with Λ as is shown in Fig. 3.

The vertical structure of the vortex core is shown more clearly by plotting W_m/V vs Z/R for $S=0.55$. This can be seen in Fig. 5. Barcilon (1967b) has presented an analytical model of the vortex core which indicates that at great heights in the vortex where the effect of buoyancy dominates over rotation, the vertical velocity decreases as $Z^{-\frac{1}{3}}$. Examination of the data shows that this dependence fits well for $Z/R>0.8$. Below this level in the vortex, where rotation plays a more important part, the velocity should decrease less rapidly with height. The analysis of Barcilon shows

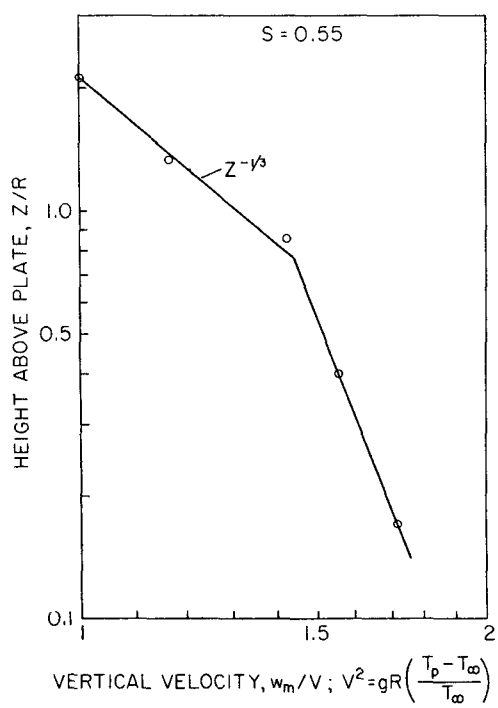

FIG. 5. Vertical velocity vs height above plate measured at five different heights above the plate for $S=0.55$. Above $Z/R=0.87$ the vertical dependence is nearly $Z^{-\frac{1}{3}}$, following the theoretical prediction of Barcilon.

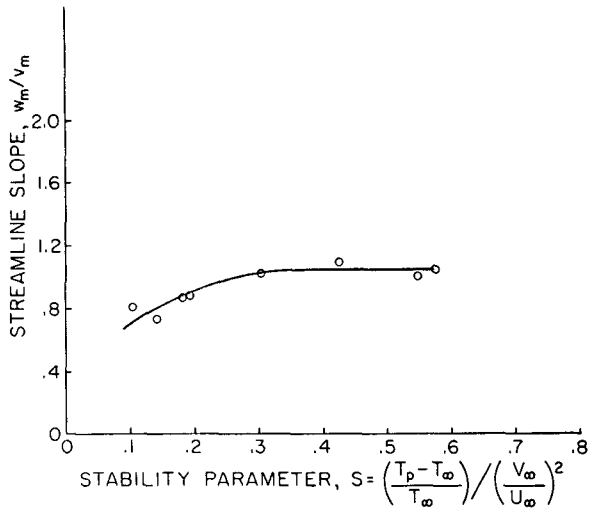

FIG. 6. Streamline slope vs stability parameter S. See text for definition of W_m/V_m.

that as we move downward toward the base of the vortex dW/dZ should become vanishingly small. This can be seen in Fig. 5 below $Z/R=0.8$. The predictions of the analysis seem to be in good agreement with the measured values of vertical velocity.

Visual inspection of the flow in the test chamber showed that the tangential and vertical velocities in the vortex core were nearly equal for most values of S. This is confirmed by the measurements shown in Fig. 6. The value of W_m/V_m is shown versus S for one value of height, $Z/R=0.41$. The result $W_m/V_m=1$ corresponds to post-vortex-breakdown "subcritical" flow and is consistent with observations of vortex breakdown at the lower surface discussed in Section 6. The measurements also show that W/V decreases at small S. This will be seen to agree with observations that significant areas of downdraft occur at the center of the vortex under the conditions of small S.

5. Temperature measurements

The thermistor probes used to determine temperature structure of the vortex core were described above. The measurement technique was similar to that used to obtain velocities. The probe was placed at a given place in the test chamber and the temperature determined by the thermistor was recorded on a strip chart. As the vortex passed over the probe the temperature excess was recorded at each level. Sufficient number of events were recorded at each level to insure that the temperature excess was representative of the operating conditions.

The results of this procedure are plotted in Fig. 7. The variation of ΔT with S is not as apparent as it was in the case of W_m/V. For this reason the mean is calculated at each level for all the different values of S. In each case the variance is approximately 0.05.

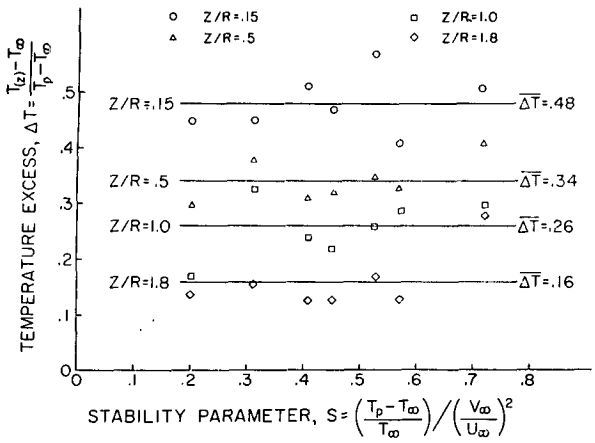

FIG. 7. Temperature excess vs stability parameter S for $Z/R = 0.15$, 0.50, 1.0, 1.8. Average temperature excess for each level is $\overline{\Delta T}$.

The vertical structure of temperature in the vortex is displayed in Fig. 8 by plotting the average temperature excess ΔT vs Z/R. The decrease of temperature with height in the upper portion of the vortex is approximately Z^{-1}, in contrast with the $Z^{-5/3}$ dependence predicted by Barcilon's theory. The theory allows no temperature stratification outside the vortex core. The temperature excess becomes just the inverse mass flux at a given level, and, as such, depends directly on the pickup parameter, which simulates the turbulent mass exchange at the outside edge of the core. The results shown in Fig. 8 indicate that the assumption of constant pickup parameter may be incorrect and the

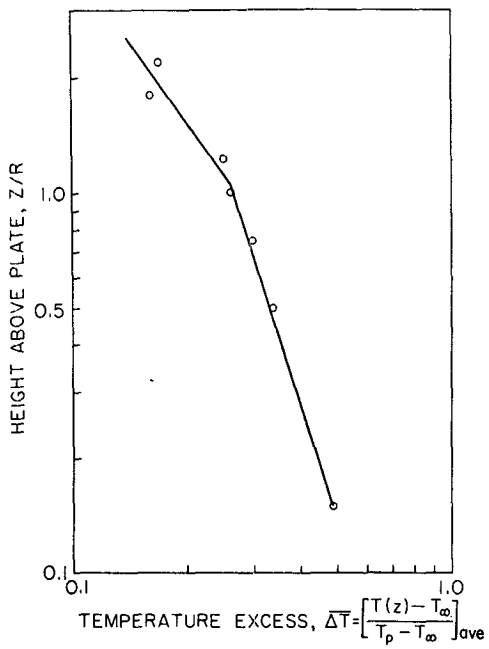

FIG. 8. Temperature excess vs height above plate, averaged over all values of S.

turbulent exchange is less at very high levels than it is farther down. It would be reasonable to expect that the turbulent exchange would become small as we go very high in the vortex; this would explain the smaller decrease of temperature with height which was observed.

6. Observations of flow patterns

Limitations of the measuring techniques described above are obvious. Because of the instruments available to make physical measurements and the complex nature of the flow field, a very incomplete picture of the flow has been obtained. It has not been possible to describe the streamline patterns in any detail at all because of the sparsity of data available. A great deal of information can be obtained by careful observation of a tracer in the flow, however.

The experimental setup which was used lends itself nicely to visual observation of the flow patterns. There is little obstruction to vision caused by the windows used to create ambient vorticity. A smoke tracer can be inserted easily into any portion of the flow field as desired.

The vortex flows can be classified into several different flow regimes, corresponding roughly with those given by Chang (1969). Very similar vortex types are also described by Ward (1970). The flow regime observed in the test chamber depends upon the particular combination of window angle and plate temperature which determine the operating condition. While the flow type descriptions are by nature somewhat subjective and classification into different types is arbitrary, the significant conditions present in the test chamber are well represented in each case.

Flow type I (no significant vortex). In this case there is very little swirl to the incoming air, so the flow in the chamber resembles that of a convective box. See Fig. 12 for the approximate range of operating conditions which produce this type vortex. Random thermal turbulence exists with its intensity depending on the temperature of the plate. If a vortex forms at the center of the chamber it is only a tiny laminar filament that is transient and very unstable. Any vortex flow which results is also very localized. Smoke which is introduced at the outer edge of the chamber does not reach the center, it merely rises under the action of convection.

Flow type II (one cell vortex). With just a bit more swirl to the incoming flow than type I, the vortex is a small laminar one but is stronger and more persistent. The diameter of the vortex is approximately 1 cm and no vortex breakdown is observed. That is, there is no stagnation point along the centerline of the vortex, and the flow in the vortex core appears to be upward at any radius. Some of the smoke introduced at the outer edge reaches the center, but the circulation is not a strong one. The flow in this regime does not appear

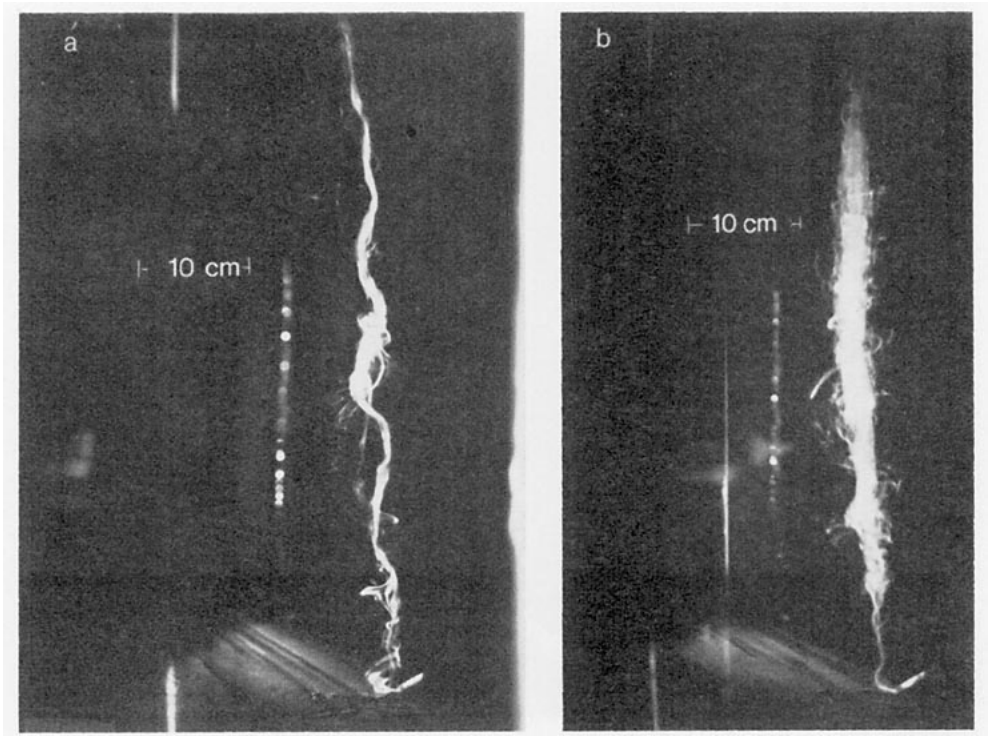

FIG. 9. Photographs of type II (a) and type III (b) vortices. The small-diameter vortex classified as type II, of the one-cell type, is seen in the laboratory test chamber as made visible by smoke. The strong vortex classed as type III has a weak downward flow at $r=0$.

to be similar to dust devils observed in the field. An example of this type of vortex is shown in Fig. 9a.

Flow type III (vortex with two-cell motion). Adding yet more rotation to the inflow (at constant plate temperature) than type II yields a vortex with much stronger circulation (Fig. 9b). A vortex breakdown is seen which oscillates up and down, generally between 2 and 10 cm above the plate (Fig. 10). The vortex breakdown appears as a stagnation point along the centerline of the flow and is accompanied by turbulence. Analyses of this phenomenon are given by Benjamin (1962), Lewellen (1971) and Bossel (1969). Below this point the vortex core has a very small diameter (1 cm) and smoke streaks in the flow have a high helix angle indicating that $W/V>1$. Above the vortex breakdown, the vortex core has a turbulent appearance, is of a large diameter (4–5 cm), and the smoke streaks indicate that $W/V\approx 1$. A quite similar description and photograph is presented by Ward (1970). The diameter is approximately constant in this region, being about 5 cm at 80 cm above the plate. The frequency of oscillation of the vortex breakdown depends on the plate temperature. It moves up and down very quickly at the higher temperatures. At times the vortex breakdown appears to move up the whole length of the vortex, leaving it a thin filament-like "supercritical" appearance. The vortex then bursts out suddenly to a larger diameter in a very turbulent manner, and the stagnation point reappears at the base near the hot plate. Above the vortex breakdown sinusoidal oscillations move up and down the vortex core and appear to whip it like a rope under tension. The wavelength of these disturbances is approximately 20 cm and their amplitude a few vortex diameters. The base of the vortex moves about randomly in a circular pattern. The radius of this movement depends on plate temperature, being about 1 vortex diameter at the higher temperatures and several vortex diameters at lower temperatures. Farther above the base plate the lateral motion is greater than at the vortex base. The motion at 80 cm above the plate is observed to be 4–5 times greater than immediately at the base of the vortex.

Maximum vertical motion in the vortex core occurs at the radius of maximum tangential motion. At the center the motion is either positive and very small or slightly negative, hence the term weak two-cell motion. By turning the smoke tracer on and off, the radial position of maximum vertical velocity can be seen clearly.

Flow type IV (vortex with strong two-cell motion). By increasing the incoming swirl (or alternately by decreasing the plate temperature) from the corresponding type III conditions, a different vortex flow is observed. In contrast with type III, the vortex breakdown region stays within 1–2 cm of the surface (Fig. 11). Downflow at the center of the vortex is substantial, and this region of downflow occupies approximately half of the whole vortex core. The vortex core is much

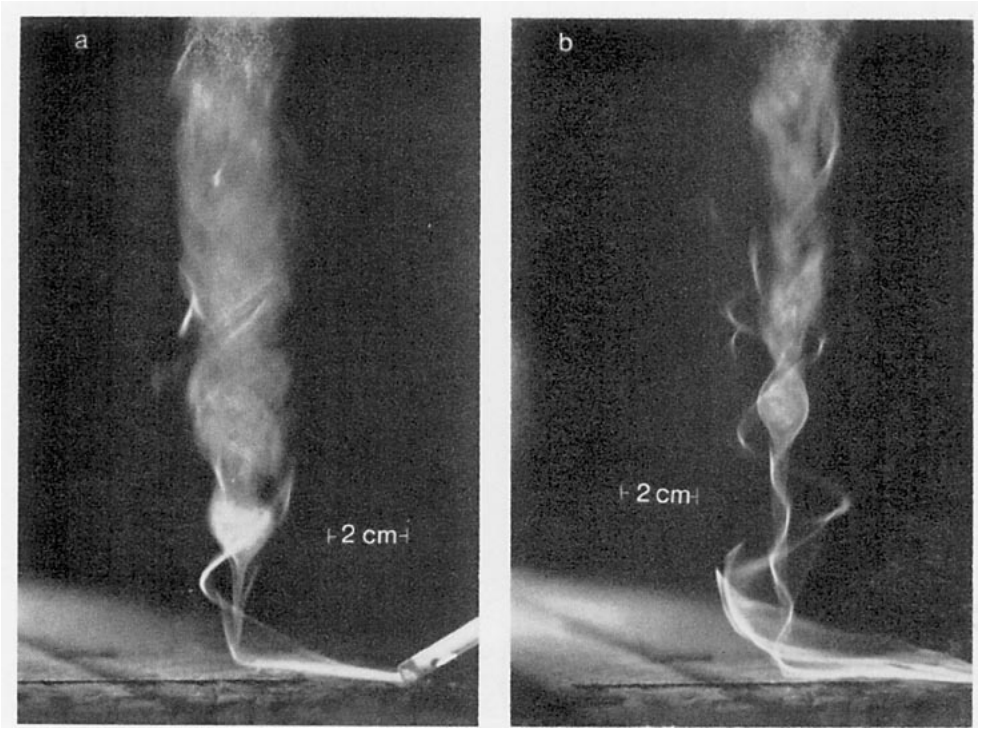

FIG. 10. Photographs of type III vortex details, showing the lower portion of the vortex. A vortex breakdown is seen in both views as a bubble of stagnated flow along the centerline. Below the vortex breakdown the smoke streak shows a high angle ($W \gg V$), and above the vortex breakdown the angle is nearly 45° ($W \approx V$). The smoke streak outside the vortex core is not affected by the vortex breakdown.

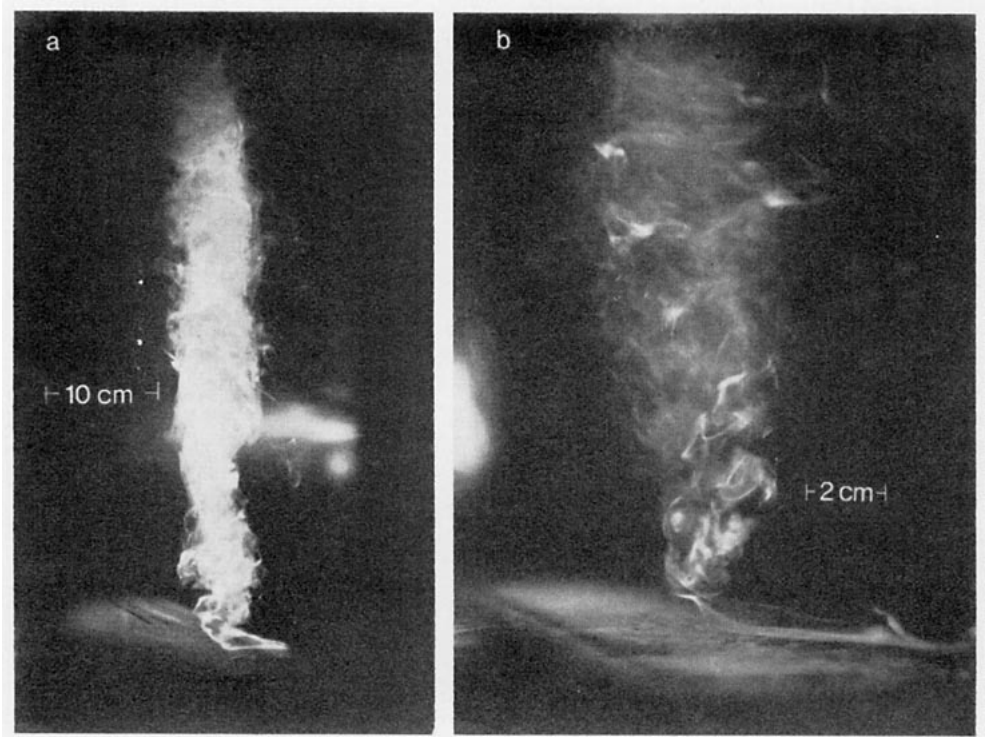

FIG. 11. Photographs of type IV vortex details. The large-diameter vortex classed as type IV is much more turbulent than type III and has a large area of downflow at the center (a). The lower portion of the vortex (b) shows the turbulent appearance; the vortex breakdown stays very close to the plate.

TABLE 3. Similarity comparison.

Source	A_∞ ($m^2\ sec^{-1}$)	$\bar{w}$ ($m\ sec^{-1}$)	r_0 (m)	Q_c ($m^3\ sec^{-1}$)	Re_t	Re_r	ϵ_c
$S=0.1$	0.0265	0.14	0.06	1.2×10^{-3}	1.6×10^3	1.2×10^3	0.76
$S=0.14$	0.0320	0.17	0.05	0.74×10^{-3}	1.9×10^3	1.1×10^3	0.58
$S=0.2$	0.0320	0.28	0.02	0.58×10^{-3}	1.9×10^3	1.2×10^3	0.60
$S=0.3$	0.0175	0.24	0.025	0.35×10^{-3}	1.0×10^3	0.8×10^3	0.80
$S=0.4$	0.0200	0.33	0.02	0.30×10^{-3}	1.2×10^3	0.9×10^3	0.76
$S=0.6$	0.0215	0.43	0.02	0.40×10^{-3}	1.3×10^3	1.2×10^3	0.93
Sinclair dust devil no. 1	78.0	7.5	3.5	108	4.5×10^6	1.8×10^6	0.40
Sinclair dust devil no. 2	117.0	5.5	5.0	162	6.7×10^6	1.9×10^6	0.29
Kaimal and Businger	36	4.0	4.0	75	2.4×10^6	1.3×10^6	0.52
Wan and Chang experiment no. 1	16.7	1.8	0.084	0.04	1.3×10^6	2.9×10^4	0.022
Wan and Chang experiment no. 2	11.0	24.2	0.076	0.44	7.1×10^5	3.6×10^5	0.51
Hoecker tornado	30100.0	$V_0=68.0$	67.0	3×10^6	4.4×10^9	2.2×10^9	0.50

more turbulent and ragged at the edges than with type III motion. Downward moving flow at the top of the vortex is especially turbulent and appears to limit the vertical extent of the vortex core. Core radius increases with height much faster than in type III motion. Radius grows from approximately 6 cm close to the base to 10 cm at 80 cm above the base. This indicates that turbulent pickup at the outer edge of the core is much larger for this case than type III. To take advantage of these observations in improving the model of Barcilon, the pickup parameter would have to be made a function of V_∞ or of the tangential Reynolds number $Re_t=V_\infty R/\nu$.

While the vortex appears turbulent and ragged at the edges in this regime, the rope-like oscillations mentioned regarding type III are not present. The vortex core remains straight and does not appear to be as susceptible to gusts as type III. The base also is more stable, remaining within half a vortex radius of the same position.

Flow type V (solid body rotation). In this case buoyancy caused by the heated plate is not sufficient to overcome rotation. A strong swirling flow includes the whole chamber, but a concentrated vortex is not formed. A large region of downflow appears at the center of the chamber, and the flow in the rest of the chamber rotates nearly as a solid body.

Flow types III and IV appear to be quite similar to dust devils observed in nature and to the two most realistic types of experimental flows described by Chang (1969). The experiment of Ward (1970) also produces similar vortices.

The effect of varying the parameters $(T_p-T_\infty)/T_\infty=\Delta T/T_\infty$ and θ is summarized in Fig. 12, which shows the relationship between the different types of flow and the governing parameters. Since the flow varies continuously between one type of flow and another, the boundary between different types of flow should be interpreted as an approximate one. The form of the results shown in Fig. 12 suggest why the stability parameter S is useful: it combines the effects of changing either variable into one quantity.

7. Comparison with non-convective vortices

To relate the observations described here to the observations given by Chang (1969), it is necessary to determine $Re_r=Q_c/(r_0\nu)$ and $Re_t=V_\infty R/\nu$, where Q_c is the mass flow rate in the vortex core, r_0 the radius of the core, and ν the kinematic viscosity. The quantity corresponding with S is $\epsilon_c=Re_r/Re_t$. The tangential Reynolds number has already been calculated and is shown in Table 1. Calculation of Re_r poses a more difficult problem, however. To make an estimate, the vertical velocity of Fig. 2 was multiplied by 0.25 to account for the fact that the velocities were peak values. They need to be averaged both across the radius of the vortex core and in time to be compared

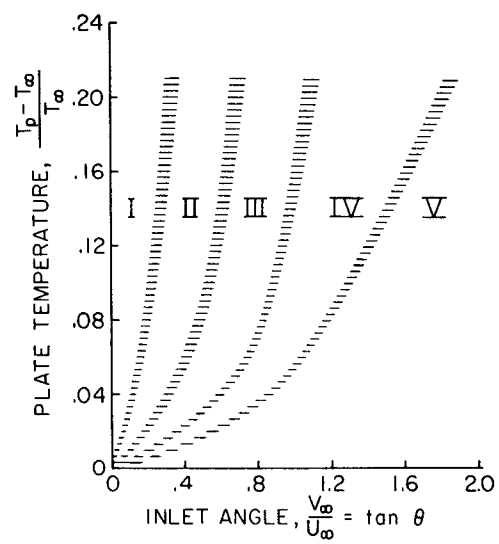

FIG. 12. Observed vortex types vs plate temperature and inlet angle, showing the dependence of observed vortex characteristics on experimental conditions.

with the field results. The region of upward motion was taken to be between r_0 and $r_0/2$ to account for the center region with no upward motion. The resulting calculations are shown in Table 3, together with the comparable figures given in Wan and Chang (1972). Also shown for comparison are the calculations for the three dust devils of Table 2 and the tornado of Hoecker taken from Wan and Chang.

We can see, in general, that increasing S is equivalent to increasing ϵ_c. The exception is the case $S=0.1$, which is one with significant downflow in the center of the vortex. Estimating Q_c becomes very difficult in this case. The values of ϵ_c obtained from the present experiment compare favorably with example No. 2 of Wan and Chang. The rough estimates involved in the above procedure preclude any detailed comparison, but it appears that both the present experiment and the non-convective experiment of Chang are dynamically similar to real dust devils.

8. Conclusions

The present experiment yields concentrated vortex flows which are similar to dust devils. Observation of the laboratory flows has helped to clarify the effects of changes in boundary conditions surrounding the vortex core. The immense variability of flow types occurring in nature has been duplicated and related to changes in these boundary conditions.

Comparisons between the results and those of Ward (1970) and Wan and Chang (1972) illustrate the effects of using different boundary conditions to drive the motion. The comparison also shows the similarities between these dust-devil-type thermal vortices and non-convective vortices designed to simulate tornadoes.

Because of the natural variability of the thermal vortex, both in position and time, the limitation of measuring only one velocity component poses a severe restraint. Future work in this area should include instruments capable of determining the temperature and three components of velocity simultaneously, thus allowing the calculation of the heat and momentum transport due to the vortex.

Acknowledgments. This work was used to satisfy, in part, the requirements for the Ph.D. degree at the Department of Meteorology, University of California, Los Angeles.

Portions of this work were completed while the author held a Regents' Graduate Internship. Additional support was provided by the Atmospheric Science Section, National Science Foundation, under Grants GA-31247 and GA-33437.

REFERENCES

Barcilon, A., 1967a: Vortex decay above a stationary boundary. *J. Fluid Mech.*, **27**, 155–175.

——, 1967b: A theoretical and experimental model for a dust devil. *J. Atmos. Sci.*, **24**, 453–466.

Benjamin, T. B., 1962: Theory of the vortex breakdown phenomena. *J. Fluid Mech.*, **14**, 593–629.

Bossel, H. H., 1969: Vortex breakdown flowfield. *Phys. Fluids.*, **12**, 498–508.

Carrier, G. F., A. L. Hammond and O. D. George, 1971: A model of the mature hurricane. *J. Fluid Mech.*, **47**, 145–170.

Chang, C. C., 1969: Recent laboratory model study of tornadoes. *Preprints Sixth Conf. Severe Local Storms*, Chicago, Ill., Amer. Meteor. Soc., 244–252.

Fitzjarrald, D. E., 1972: The dust devil: A laboratory and field investigation. Ph.D. dissertation, Dept. of Meteorology, UCLA.

Kaimal, J. C., and J. A. Businger, 1970: Case studies of a convective plume and a dust devil. *J. Appl. Meteor.*, **9**, 612–620.

Kuo, H. L., 1966: On the dynamics of convective atmospheric vortices. *J. Atmos. Sci.*, **23**, 25–42.

Lewellen, W. S., 1962: A solution for three-dimensional vortex flows with strong circulation. *J. Fluid Mech.*, **14**, 420.

——, 1971: A review of confined vortex flows. NASA CR-1772.

Long, R. R., 1958: Vortex motion in a viscous fluid. *J. Meteor.*, **15**, 108–112.

Maxworthy, T., 1964: The flow-creating a concentration of vorticity over a stationary plate. *Space Programs Summary Jet Propulsion Lab.*, **4**, 37–44.

Serrin, J., 1972: The swirling vortex. *Phil. Trans. Roy. Soc. London*, **A271**, 325–360.

Sinclair, P. C., 1966: A quantitative analysis of the dust devil. Ph.D. dissertation, Dept. of Meteorology, University of Arizona.

Turner, J. S., and D. K. Lilly, 1963: The carbonated-water tornado vortex. *J. Atmos. Sci.*, **20**, 468–471.

Wan, C. A., and C. C. Chang, 1972: Measurement of velocity field in a simulated tornado-like vortex using a three-dimensional velocity probe. *J. Atmos. Sci.*, **29**, 116–127.

Ward, N. B., 1970: The exploration of certain features of tornado dynamics using a laboratory model. NOAA Tech. Memo. ERLTM-NSSL 52.

Ying, S. J., and C. C. Chang, 1970: Exploratory model study of tornado-like vortex dynamics. *J. Atmos. Sci.*, **27**, 1–14.